Molecular-dynamics simulations of electronic sputtering

E. M. Bringa and R. E. Johnson
Engineering Physics, University of Virginia, Charlottesville, Virginia 22903

M. Jakas
Engineering Physics, University of Virginia, Charlottesville, Virginia 22903
and Departamento de Física Fundamental y Experimental, Universidad de La Laguna, 38201 La Laguna Tenerife, Spain
(Received 11 May 1999)

Following electronic or collisional excitation of a solid by a fast ion, an energized cylindrical region is produced which can lead to sputtering. Here ejection from such a region is studied via molecular-dynamics simulations using Lennard-Jones and Morse potentials. Over the full range of excitations studied the yield vs the energy release per unit path length in the solid, which we call dE/dx, is shown to scale with the binding energy and with the density of the material for all materials studied and at all dE/dx. This allows the simulation results to be applied to low-temperature, condensed-gas solids and to more refractory solids over a broad range of dE/dx. The effect of a distribution of energies for the initial energizing events, and the effect of a spatial distribution of such events for a given dE/dx are examined. Three regimes have been identified. When the energy release per excitation event is greater than the escape energy, sputtering is linear in dE/dx at low dE/dx. With increasing dE/dx a spikelike regime occurs in which the yield again becomes nonlinear with dE/dx. For *fixed* cylindrical radius ejection then saturates so that at very high dE/dx the yield again becomes nearly linear with dE/dx. In this regime the size of the yield increases with the initial radial extent of the track and is determined by the removal of energy radially by the pressure pulse and by the transport of energy from depth to the surface. Therefore, the clear nonlinearities observed in the knock-on sputtering yields by heavy ions require consideration of the radial extent of the cascades. For electronic sputtering yields of condensed-gas solids, the observed nonlinearity in the sputtering yield suggests that the radial extent of the excited region varies in a manner different from that predicted or that the energy release to the lattice is nonlinear in the stopping power. [S0163-1829(99)02146-3]

I. INTRODUCTION

In two recent papers[1,2] (hereafter I and II) molecular-dynamics (MD) simulations of a cylindrically energized region were carried out in order to describe the transport of energy from a track of excitations produced by a fast ion and to test ''thermal'' spike models for sputtering. Although spike models have been used for over 50 years to describe the nonlinear aspects of sputtering,[3,4] ion-beam induced mixing,[5,6] and track formation[7,6] by fast ions, there have been relatively few tests using atomistic simulations. One of our goals is to understand the applicability of spike models to laboratory results on the electronic sputtering of low-temperature condensed-gas solids.[8–10] Such experiments provide one of the few means of determining the nonradiative electronic relaxation pathways in molecular insulators.[8,9,11] The electronic sputtering of low-temperature ice is also of interest as it produces atmospheres on the moons of Jupiter.[12]

Laboratory studies of fast ions incident on low-temperature condensed-gas solids show that the yields for the molecular solids all exhibit a roughly quadratic dependence on dE/dx at high dE/dx. Here dE/dx is the energy deposited per unit path length by a fast ion and is also called the stopping power.[13] Spike models, in which the energy transport is diffusive, also give yields quadratic in dE/dx for the cylindrical geometry appropriate to fast ions. In such models, of course, dE/dx is the kinetic energy per unit path length of the moving atoms or molecules in the spike. Assuming this value of dE/dx is proportional to the stopping power, the laboratory observations have been parametrized using spike models.[14] This parametrization allows one to beautifully scale data for different targets over a broad range of dE/dx.[14] However, we found to our surprise that the yield calculated using MD simulations for initial conditions associated with a spike is *not* quadratic in dE/dx for those values of dE/dx appropriate to the nonlinear electronic sputtering regime.[15,2] Quite remarkably, the sputtering yields calculated using MD for fixed track radius are nearly linear in dE/dx at high dE/dx *even though* the transport processes are *clearly nonlinear*. That is, above some ''threshold'' value of dE/dx saturation sets in unlike in the analytic spike models. We showed that the difference in the dependence of the yield on dE/dx obtained in the MD simulations from that dependence obtained using a spike model is *not* due to a lack of thermal equilibration locally in the rapidly evolving spike, and we showed earlier that local equilibration was *not* required in order to obtain the quadratic dependence of the yield.[14] In addition, Jakas[16] showed that the quadratic dependence in spike models in which the energy transport is diffusive is robust since it persists even when realistic thermal properties which allow melting are used rather than the analytic model properties typically used.

The difference between our MD simulations and the spike models is due to two factors. First, the energy transported away from the excited cylindrical region at high dE/dx cannot be described diffusively but is more closely

described by a pressure pulse at large radii and a melt at small radii.[1,17] Second, the presence of the surface affects the energy flow[2] in a way that differs from available spike models.[18] At high dE/dx these transport processes act to produce a yield which increases nearly linearly with increasing dE/dx for fixed track radius. This surprising result is expanded upon here and made much more general. In doing this we show that the MD results are applicable to a broad range of interesting materials. The results are shown to be general by considering factors that could affect the dependence of the yield on the stopping power in the MD calculations and certainly affect the relevance of the results to a range of materials.

II. CALCULATIONS

In paper II and earlier works, the energy transport and sputtering yields were initiated by fully exciting a cylindrical region in a solid described by molecular dynamics. The region is intended to represent a track of nonradiative relaxation and energy transfer events following the passage of a fast, heavy ion. These calculations were carried out for both atomic and molecular solids in paper II, and were carried out for amorphous solids in the earlier calculations.[15,19–21] In the other extreme, MD simulations have been carried out for energy transport and sputtering produced by an individual, nonradiative relaxation events or energy transfer events randomly placed in the solid. Again results have been obtained for both atomic and molecular solids which are either crystalline or amorphous.[19,22–25] For the kinetic energy densities studied, parametrized by dE/dx and the track radius $r_{\rm cyl}$, it was found that the character of the results is roughly the same for atomic and molecular solids and for crystalline and amorphous solids.

In papers I and II Lennard-Jones (LJ) potentials were used to construct the MD solids. Because the equations of motion can be *fully scaled* using the two LJ parameters, the calculated yields could also be scaled to solids other than that studied. This useful result should be treated cautiously since, although the LJ potential is probably applicable to the condensed-gas solids, it gives a very poor description of properties for most other materials. To extend our analysis to a broader range of materials, including refractory solids, we repeat the key calculations in II using a Morse potential. This potential has three scaling parameters allowing it to better fit material properties.[26,27] By choosing the Morse potential we have a potential form which can be used to describe a broader range of materials but is still general, rather than having a specific potential for each material. More complex potentials are easily incorporated, but we choose a simple form to allow us to continue to investigate the aspects of collisional energy transport and sputtering common to a number of solids.

Here the Morse potential is used for a large range of material parameters. We again find that the energy transport from the cylindrically excited region is *not* diffusive, but is more closely described by a pressure pulse, and we again find that in the *nonlinear energy transport* regime (dE/dx large) the sputtering yield vs dE/dx for fixed $r_{\rm cyl}$ is linear for *all* materials contrary to spike model predictions. Indeed we find the very useful result that the yield vs dE/dx can *still be scaled* using the parameters of the potential. This allows our earlier results, and the new results here, to be applicable to more refractory solids at high dE/dx. Therefore, the sputtering calculations apply to a broad range of materials and incident ion energies and types. In addition, we show that the sputtered-particle energy distributions from a track of excitations in the nonlinear regime can exhibit a dependence close to that typically found in linear collision-cascade sputtering, even though the conditions for the linear cascade *do not* apply. The energy dependence of the ejecta also scales with material properties using the potential parameters.

Because the initial distribution of events can affect the yields we consider a more realistic distributions here. In papers I and II all of the atoms or molecules in the cylindrical track were excited in order to most closely represent the initial conditions in spike sputtering and, thereby, test ''thermal'' spike models. Because a fast ion, in fact, creates a distribution of excitation or energy transfer events along its path, we describe in this paper sputtering produced by a spatial distribution of energy release events determined by the value of dE/dx. In isolation each such event would separately produce a minicascade of moving atoms.[22,23,25] The use of a spatial distribution, rather than a fully excited cylindrical region, primarily affects the dependence of the yield at low dE/dx where the distribution is sparse. As dE/dx increases the number of events per unit path length also increases until the excitations begin to interact, creating a region in which a large number of moving atoms collide among themselves forming a cylindrical spike.[14] The transition from isolated excitations to the fully excited track is calculated here for a number of track widths. This transition is particularly relevant to the electronic sputtering of O_2 and N_2. The *measured* yields for both of these materials exhibit a striking change in dependence on dE/dx in going from low to high dE/dx,[14,28] whereas the results for the assumed track width do not. Spikelike effects have been observed in MD simulations of self-bombardment of Au,[29] where flow of liquid material to the surface was shown. A viscous flow model was proposed to account for this, also predicting a quadratic dependence of the yield with dE/dx.[29]

Finally, we analyze the influence on the calculated sputtering yield of incorporating a distribution of velocities for each excitation event. As in earlier work,[15,19,22] we have typically used a single energy per atom at each dE/dx, which we call a δ function distribution.[14,28] This was done both for convenience and because equilibration is fast. For a knock-on event in the sputtering of a refractory material, or a nonradiative relaxation following an electronic excitation, there is a distribution of ''initial'' energies. Because we continue to be interested in testing spike models, we use a Maxwellian distribution here to describe the initial energies. The yields so calculated are compared to those for the δ distribution. A Maxwellian, of course, applies when full equilibration occurs locally. In paper I we showed that equilibration within a uniformly excited region occurred in approximately one collision time. The equilibration is rapid in a solid because an energized particle interacts simultaneously with many neighbors. However, when the excited track is surrounded by cold material the radial energy transport competes with equilibration and quasiequilibration locally can require picoseconds.[2] Since sputtering also takes picosec-

TABLE I. Morse potential parameters for Ar and Cu.

	D (eV)	r_o (Å)	α (Å^{-1})	$r_{\rm cut}$ (Å)	$n_o r_o^3$	m (10^{-26} kg)
Ar	0.0118 (1)	3.82 (1)	1.56 (5.96)	8.52 (2.23)	1.489	6.69 (1)
Cu	0.3593 (1)	2.813 (1)	1.3534 (3.81)	5.25 (1.87)	1.885	10.56 (1)

onds, we find here that differences between the Maxwellian and δ distributions occur at low dE/dx, affecting the ''threshold'' dependence for a cylindrical spike but not the yields at high dE/dx. We also find that in this ''threshold regime'' the analytic diffusive spike models can fit the MD simulations.

III. SIMULATION DETAILS

As in previous papers, for many of the calculations carried out here we use a Lennard-Jones (6-12) potential $V(r) = 4\varepsilon[(r/\sigma)^6 - (r/\sigma)^{12}]$ with a cutoff radius $r_{\rm cut} = 2.5\sigma$ to describe an fcc solid. This cutoff radius includes up to fifth nearest neighbors for a density $n = 0.0265$ Å^3 (a total of 78 neighbors). The values $\varepsilon/k_B = 119.8$ K and $\sigma = 3.405$ Å used in the simulations were those for solid Ar. The sample has a binding energy $U = 0.08$ eV and a (001)-layer spacing $l = 0.78\sigma$. The surface binding energy is $U_s = 0.055$ eV for the (001) surface. Because the equations of motion can be fully scaled using the two LJ parameters, results for the yield and sputtered atom properties for other Lennard-Jones (LJ) solids can be obtained by scaling with l and U. More details on the LJ calculations can be found in paper I. The local kinetic temperature of the atoms and molecules, $T(r,t)$, was calculated for a cylindrical shell of mean radius r, as explained in paper II.

Here we also present results obtained using Morse potentials, $V(r) = D\{\exp[-2\alpha(r-r_o)] - 2\exp[-\alpha(r-r_o)]\}$. The minimum of the potential is located at r_o, D is the well depth, and α is related to the well width and gives the stiffness of the potential. The larger α the steeper the potential at small distances. For an fcc lattice, the lattice parameter a is related to the density by $n = 4a^{-3}$, and the nearest-neighbor equilibrium distance is $d_{\rm nn} = a/\sqrt{2}$, which is close to r_o. For specific materials there are two-body or many-body potentials that give a better description of the material's properties. However, here we choose to use Morse or LJ potentials that follow some simple scaling laws and are flexible enough to give a reasonable description of a wide range of materials. In the energy range of interest the Morse potential gives realistic collisional transport for the rare-gas solids (RGS).[22,23] Although the Morse potential is more flexible it still cannot describe all of the principal material parameters. Therefore, in the literature there are several fits to the Morse potential parameters, depending on the properties which were chosen to be fit and depending on the number of nearest neighbors considered. For rare-gas solids a constraint on key parameters is given by $\alpha r_o \approx 6$, while for metals this is typically, $\alpha r_o \sim 2-4$. Since metals have a wider potential well, it is energetically favorable to locate many particles within the well, at distances smaller than r_o. This means that the equilibrium densities ($n r_o^3 \sim 2$) are higher than those for RGS ($n r_o^3 \sim 1.5$).

It is important to notice that some potentials determined by fitting the Morse parameters to experimental values do not have an energy minimum at the experimental density. Therefore, a crystal made of atoms interacting through this potential will expand or contract if periodic boundary conditions (PBC's) are not applied. Since sputtering requires at least one free surface, theses potentials are inadequate. We used the freeware program GULP (Ref. 30) to fit the Morse potential for Cu and for Ar to three parameters: equilibrium density at 0 K (n_o), binding energy (U), and bulk modulus at zero pressure and 0 K (B). The initial values for the fitting of Cu were the ones giving by Girifalco and Weizer,[26] with a cutoff at 5.25 Å. For Ar we used the initial values from Cui.[22]

The parameters obtained for the potentials are included in Table I . The dimensionless values are indicated in parentheses, where distances are scaled with r_o and energies are scaled with the well depth D. The potential for Cu included up to fourth nearest neighbors (54 atoms), and the potential for Ar included up to fifth nearest neighbors (78 atoms). MD simulations of crystallites with free boundary conditions (FBC's) relaxed only slightly from the crystallites simulated using PBC.

Table II gives the fitting parameters and other information like elastic constants of the simulated materials, c_{ij}. Experimental values are indicated in parentheses when different from the simulated values. The experimental values of the elastic constants for Ar (Ref. 31) and for Cu (Ref. 32) are included. If only central forces are considered, $c_{12} = c_{44}$.

In order to calculate the energy transport and sputtering from a cylindrically excited region of radius $r_{\rm cyl}$, each nonradiative de-excitation event was simulated by giving an atom a kinetic energy $E_{\rm exc}$ in a random direction. Here, as in papers I and II we call dE/dx the total kinetic energy release per unit length in the cylinder. Often, the symbol $(dE/dx)_{\rm eff}$ has been used for the energy release per unit path length. This is usually presumed to be proportional to the true stop-

TABLE II. Fitting parameters (n_o, U, and B) and calculated properties of simulated materials. Experimental values are indicated in parentheses.

	n_o (Å^{-3})	U (eV)	B (GPa)	c_{11} (GPa)	c_{12} (GPa)	c_{44} (GPa)	d_{nn} (Å)
Ar	0.0267	0.08	2.7	0.37 (0.53)	0.22 (0.135)	0.22 (0.16)	3.755
Cu	0.0847	3.49	140	1.918 (1.79)	1.14 (1.26)	1.14 (0.84)	2.556

ping power of the material but, of course, does not have to be. Here we drop the subscript and our dE/dx is equal to $N_{\rm exc}E_{\rm exc}/l$, where $N_{\rm exc}$ is the average number of excited particles per layer in the track of radius $r_{\rm cyl}$. For the fully excited cylinder we can write $dE/dx \approx n\pi r_{\rm cyl}^2 E_{\rm exc}$. For a LJ potential $r_{\rm cyl}=0.8\sigma$, 2σ,5σ correspond to $N_{\rm exc}=2$, 12, 62, respectively.

The mean number of atoms ejected per run for a given set of energy release events is called the yield. Particles are sputtered (ejected) if they cross a plane at a distance $2r_{\rm cut}$ above the surface. Only results for the (001) surface are shown. Earlier we showed the yield for the (111) surface is smaller (80–70 %) but has similar features.[2] The sample size and simulation times were varied according to the size of $E_{\rm exc}$ and $r_{\rm cyl}$ as explained in previous papers.[2,23] Average yields are then calculated. The results for the yield and ejected atom properties were averaged over different random directions of the initial velocities, over the velocity distribution when the delta distribution was not used, and over different spatial distributions of excited particles when only a fraction of the particles were excited.

IV. EXCITATION REGIMES

A fast ion penetrating a solid creates a track of excitations along its path through the material. The individual events release energy which can lead to sputtering and are described by a yield Y. Here we write the number of energy transfer or nonradiative decay events per unit path length as λ^{-1}, which we assume is proportional to the incident ion's stopping power. These events are distributed randomly along a cylindrical region about the ion's path through the solid with a mean spacing λ and a mean radius $r_{\rm cyl}$. For electronic excitations $r_{\rm cyl}$ is usually determined by the ion velocity.[28] There are two limiting cases that have been studied using MD. First, a sparse distribution, in which energy release from the individual events disperses separately (very low dE/dx). In this limit the total yield can be written as the probability that an event occurs close to the surface.[33,22] In the other limit, a high density of excitations, there are many excitations per monolayer so that all particles within the track are excited and the transport of energy from the individual events cannot be treated as independent[8,2]. In the simulation dE/dx can increase either by increasing the energy per event, $E_{\rm exc}$, with fixed $r_{\rm cyl}$, or by increasing $r_{\rm cyl}$. For electronic sputtering, for instance, the amount of energy needed to produce an electron-hole pair in Ar is $W=23.6$ eV. A 0.5 MeV He^+ ion going through Ar has $dE/dx=21.3$ eV/Å (calculated from TRIM98) giving a mean free path for producing an electron-hole excitation $\lambda = W/(dE/dx) = 1.11$ Å (2.4 excitations per layer). If we take the radius of the track core to be the Bohr adiabatic radius,[34] then $r_{\rm cyl}=h\nu/(2W)=4.35$ Å$=1.3\sigma$, so every atom in the cylindrical region is energized, ignoring excitation transport. On the other hand a 6 MeV H^+ ion going through Ar has $dE/dx=0.75$ eV/Å , giving a mean free path for producing an excitation, $\lambda=31.47$ Å (1 excitation every 12 layers). The radius of the track is $r_{\rm cyl}=14.84$ Å$=4.3\sigma$, so the cylindrical region is sparsely excited. In this case the individual events essentially relax separately. In laboratory studies of solid N_2 and O_2 the incident ion energy and type was varied to study the transition between these limiting cases. The electronic sputtering yield was found to vary from linear to very nearly quadratic in the stopping power as mentioned earlier.[14]

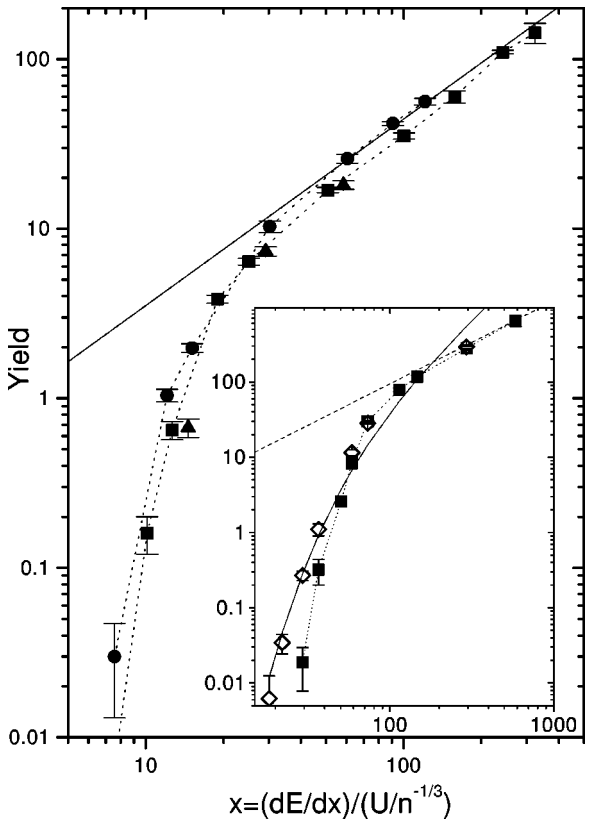

FIG. 1. Yield for $N_{\rm exc}=12$ as a function of scaled dE/dx. LJ Ar (squares), Morse Ar (triangles), and Morse Cu (circles). $Y \propto (dE/dx)^{1.1}$ (solid line), is included to guide the eye. Inset: Yield for $N_{\rm exc}=62$ as a function of scaled dE/dx for LJ Ar. δ distribution (solid squares), Maxwellian distribution (open diamonds). SC thermal spike model is given by a solid line. $Y \propto (dE/dx)^{1.1}$ (dashed line), is also included.

A. Fully excited track

When every atom or molecule within the cylindrical track of radius $r_{\rm cyl}$ is given an excitation energy $E_{\rm exc}$, it has been shown that the resulting yield can be written as $Y \propto (dE/dx)^n$. Two regimes are found in the MD simulations. When $E_{\rm exc} \leqslant U$ there is a steep ($n \geqslant 3$) *threshold regime* that exhibits aspects of a spike as the atoms or molecules must collide and gain energy to overcome the potential energy barrier.[2] When $E_{\rm exc} > U$ there is a *high* dE/dx regime with $n \approx 1$ for both crystalline[2] and amorphous[15] solids. *Both* the threshold regime and the high dE/dx regime differed in their dependence on dE/dx from the spike-model predictions.

We repeated these studies here using a Morse potential that gives the same nearest-neighbor distance and the same sublimation energy for solid Ar. In addition, we have used those Morse parameters appropriate for a *refractory* solid, Cu. Because of its much larger sublimation energy, up to 28 eV of energy per atom had to be used for Cu, whereas in Ar only a few eV per atom were used. In Fig. 1 the yields vs dE/dx for fixed $r_{\rm cyl}$ are presented along with the earlier results for an LJ solid, calculated for Ar.[2] Because the equa-

tions of motions can be completely scaled using the two LJ parameters, the yield vs dE/dx can also be scaled using those parameters. However, there are two length parameters in the Morse potential, therefore, the *equations of motion* cannot be simply scaled. In spite of this, we show in Fig. 1, that plotting Y vs the scaled stopping power, $(dE/dx)/(U/n^{-1/3})$, the yields for *all* the simulations fall very nearly on the same curve. This surprising result indicates that for atomic solids the yield scales between very different materials in a way that does not depends on the details of the potential. Therefore, the work in paper I can apply to a broad range of solids. In addition, if our MD calculations for the sputtering of solid O_2 (paper II) are scaled by U and $n^{-1/3}$, or the results for amorphous materials are so scaled for the same $r_{\rm cyl}$, they also fall roughly within this data set. The yields in Fig. 1 are all for $r_{\rm cyl}=2\sigma$, increasing $r_{\rm cyl}$ increases the yield. At high dE/dx the yield at a fixed $r_{\rm cyl}$ was shown to be nearly linear in dE/dx but the magnitude scaled roughly as $r_{\rm cyl}^n$ with $n\sim 0.8$ for a crystalline sample.[2]

Earlier it was shown that the details of the potential do not affect cascade damage and defect production under ion bombardment.[35] Simulations of collision cascades in Si using a Tersoff potential and a Stillinger-Weber potential gave very similar results, even though these two potentials are quite different.[36] The extent of phase transitions and defect distribution can differ for different potentials, like the size of the molten region in our simulations of thermal spikes, but the size of the yield is not greatly modified. It has also been shown that there *are* differences in the energy transport when using an LJ vs a Morse potential. The steeper repulsive core means that focused, nearest-neighbor collisions are *more* important for the LJ potential.[22,2] Therefore, energy and angular distributions *are* slightly different. [Ejecta distributions for Cu and $E_{\rm exc}=6U$ are given in Appendix A.] Shapiro and Tombrello[37] examined the effect in sputtering of using a many-body embedded-atom potential for Cu instead of a Morse potential. They found differences *only* in the energy and angular distributions of the ejecta and in dimer ejection. Therefore, use of the Morse potential in the present context is valid. The role of changing potential parameters has also been explored in defect creation in metals by using Cu and another Morse material with $\alpha=6$. The formation process was found to be different.[38] However, we find here that the sputtering yield *simply scales with U and* $n^{1/3}$. This is the same scaling found for linear cascade sputtering[50] and in spike models. Here it applies also when the energy transport is very nonlinear.

The threshold seen in Fig. 1 for the fully excited cylinder occurs when $E_{\rm exc}<U$. If the δ function distribution is used an atom needs to make collisions to gain enough energy to escape, hence, a thermal effect might be expected. However, the dependence in Fig. 1 [$(dE/dx)^n$ with $n\sim 6$] also differs from the quadratic dependence usually taken for the analytic[4,3] or complete[16] spike models. Thermal spike models typically assume that local equilibrium occurs very rapidly. Therefore, at every point in the energized region the atoms or molecules exhibit a Maxwellian distribution of velocities determined by the local temperature. This assumption in the analytic spike models leads to a steeper dependence at $E_{\rm exc}<U$ of the form $Y\approx T_o^n \exp[-U/(k_B T_o)]$, where $T_o\propto dE/dx$ is the initial temperature of the spike,[2] and $n=2$ for the Sigmund and Claussen (SC) model.[3] To evaluate the influence of the velocity distribution on the sputtering yield, we compare simulations made using a δ distribution, in which all particles are given the same energy, with simulations in which the initial energies are chosen from a Maxwellian distribution with the same mean energy. Earlier, Johnson *et al.*[14] compared the *analytic* spike models using the two distributions and found a shift in the threshold and a lower yield when the δ distribution was used.

The inset in Fig. 1 shows MD calculations of the yield using initial energy distributions which are Maxwellian for the case $N_{\rm exc}=62$. The details are given in Appendix B. For $E_{\rm exc}>U$ the yields are seen to be essentially identical to those calculated using a δ distribution, although the energy distribution of the ejecta differ slightly as described in Appendix B. By contrast, for $E_{\rm exc}=0.5U$, the Maxwellian yield is three times larger. These results can be understood as follows. When $E_{\rm exc}\ll U$ collisions must occur to cause ejection when using a δ distribution, but for a Maxwellian there is always the probability an atom at the surface will have sufficient energy to escape. Therefore, in comparing to spike models care must be taken in the threshold regime. *However*, when $E_{\rm exc}\gtrsim 2U$ the number of atoms escaping is *not* affected by the initial energy distributions. Therefore, the above calculations show that the nearly linear dependence of the yield on dE/dx is *not* affected by changing the potential *nor* is it affected by changing the initial energy distribution implying it is a very general result. Unfortunately, in the threshold regime there is no comparison between many-body potentials and two-body potentials, like the one mentioned above[37] for large dE/dx, so results could differ for many-body potentials.

In comparing this regime to the SC version of the analytic spike model,[3] we find that the dependence on dE/dx is nearly the same: Fig. 1 inset. Although the analytic models do not treat the surface correctly, as discussed below, this comparison shows that the radial diffusive energy transport assumption can be valid in this regime, as suggested in paper II.

B. A distribution of excitations

For the results presented in Fig. 1 the energy per event was assumed to increase with increasing dE/dx as in a spike model for fixed initial $r_{\rm cyl}$. However, when a track is energized by an incident ion, either collisionally or by nonradiative decay of electronic excitations, the spatial distribution of events varies with dE/dx at low dE/dx but the mean energy per event remains roughly constant. Therefore, we consider a distribution of excitations at low dE/dx. If $E_{\rm exc}\ll U$ sputtering requires collisions. When dE/dx is small *but* $E_{\rm exc}>U$ ejection can occur if the incident ion creates an event close to the surface. This is thought to be the case in the electronic sputtering of O_2 and N_2 (Ref. 14) at low dE/dx and it is the basis for knock-on sputtering of all solids in the linear cascade regime. Therefore, we have carried out simulations for sputtering following the production of a spatial distribution of events by a fast ion. In these simulations, each event releases $E_{\rm exc}>U$.

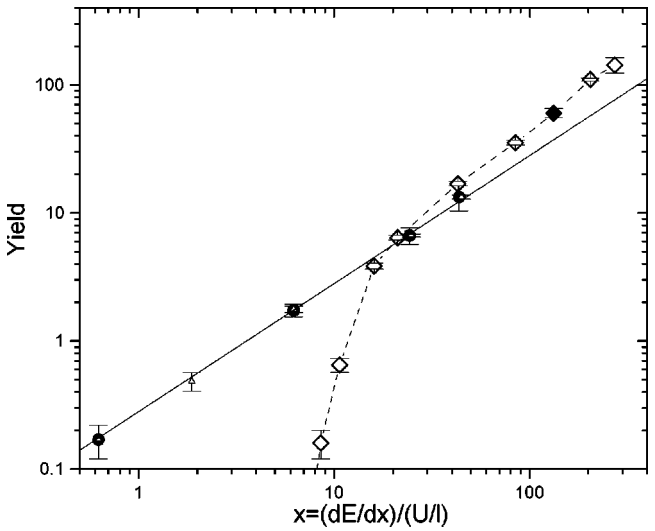

FIG. 2. Yield for a partially excited cylinder with $E_{exc}=1$ eV: $r_{cyl}=0.8\sigma$ (triangles), and $r_{cyl}=2\sigma$ (solid circles). The linear fit is $Y=0.28x$, where $x=(dE/dx)/(U/l)$. Results for a fully excited cylinder with varying E_{exc} are also included: $r_{cyl}=2\sigma$ (diamonds-dashed line).

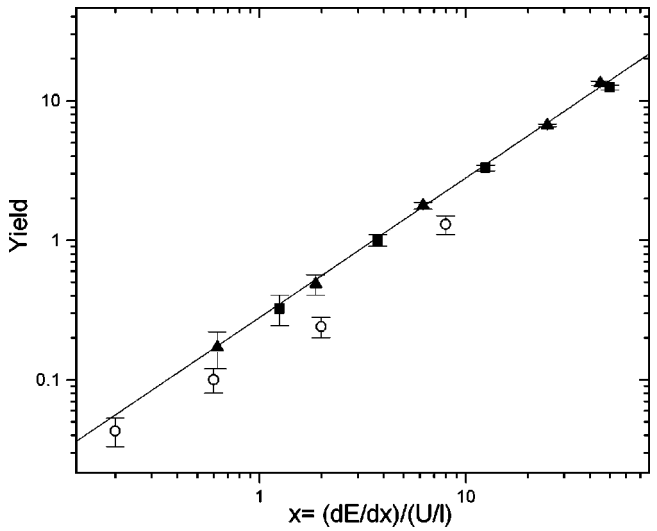

FIG. 3. Yield for partially excited cylinder with $r_{cyl}=0.8\sigma$ and different excitation energies, $E_{exc}=0.32$ eV (circles), 1 eV (triangles), and 2 eV (squares). The linear fit is $Y=0.28x$, where $x=(dE/dx)/(U/l)$.

Calling λ the mean free path for producing excitations, the yield exhibits a simple dependence on dE/dx for $\lambda \gg l$.[33,22,23] Writing the energy release per unit path length as $dE/dx=E_{exc}/\lambda$, the average yield Y is

$$Y \approx C\left(\frac{l}{\lambda}\right)\left(\frac{E_{exc}}{U}\right)=C\frac{dE/dx}{U/l}. \tag{4.1}$$

This expression exhibits the expected linearity at very low dE/dx and is discussed in Appendix C. C in Eq. (4.1) depends weakly on the interaction potential. If l is the separation between layers, $C\approx 0.28$ for the (100) surface for LJ Ar.[23] Often $l=n^{-1/3}$ is used, as in Fig. 1, changing the size of C.

When λ is small, there is a high probability that a number of energy transfer events occur close together producing nonlinear energy transport. Therefore, one might also expect that the dependence on dE/dx in Eq. (4.1) would change. To simulate this, a number of atoms within the MD track were chosen at random and energized. Average yields for 1,2,5, . . . events distributed randomly in cylinders of radius $r_{cyl}=0.8\sigma$ and $r_{cyl}=2\sigma$ were calculated in solid Ar for $E_{exc}=1$ eV using a LJ potential. These are plotted in Fig. 2 vs the appropriate dE/dx. Also shown are the results for the same cylinder fully excited. For low dE/dx and $E_{exc}\gg U$ there is no longer a spikelike threshold, as expected. At low dE/dx the yield in Fig. 2 is described by Eq. (4.1) and is independent of the radius of the cylinder. For fixed E_{exc} and fixed r_{cyl}, the yield exhibits a slight nonlinearity with dE/dx when the cylindrical region becomes nearly fully excited. The onset and size of this effect depends on the sizes of E_{exc} and r_{cyl}. Figure 3 shows the yield for $r_{cyl}=0.8\sigma$ but with different excitation energies, $E_{exc}=0.32$, 1, 2 eV ($>U$). The results fall on a line, except for the lowest E_{exc} (0.32 eV $=4U$) which approaches the effective escape energy $\sim 2U$.[23]

When a particle penetrates a solid there is, in fact, a distribution in the number of events *in a fixed sample length* for each λ. Writing the yield calculated above for each of the distribution of events as Y_I, then for a given λ^{-1}, each Y_I has a weight w_I giving an average yield, $Y=\Sigma w_I Y_I$. For a fast ion with a large penetration depth, w_I in the near surface regime is determined by Poisson statistics for constant λ. That is, when λ is such that the *average* number of events in our sample is 3, this implies weighted contributions from 1, 2, 3, 4, . . . , etc., events in the sample. This produces fluctuations in dE/dx. Such a calculation was carried out earlier[14] treating the energy dispersal from each event diffusively as in a spike model. In plotting the yield versus dE/dx in Figs. 2 and 3 the Poisson weights should be used at each dE/dx. Since the yield for each r_{cyl} and E_{exc} is nearly linear in dE/dx, the Poisson weighting will not affect the dependence of the yield on dE/dx. Therefore, the results in Figs. 2 and 3 are directly applicable to the sputtering problem.

V. CONCLUSIONS

The surprising result that the spike model for sputtering, which has been extensively used to describe nonlinear sputtering yields at high dE/dx, in fact appears to saturate, so the sputtering yield becomes nearly linear in dE/dx at high dE/dx,[2,15] is explored further here. In this paper we focused on testing the generality of the earlier calculations, by examining a number of aspects that can affect the calculation of the sputtering yield. In these comparisons we separated the sputtering process into distinct regimes based on the local energy density.

We first showed that over a broad range of dE/dx the calculated sputtering yield follows scaling laws that are very insensitive to the nature of the potential. This is the case even for more refractory materials like Cu. Therefore, although our motivation has been electronic sputtering, the results obtained in paper II and those given here can, in principle, be applied to knock-on sputtering by fast ions *if*

appropriate values of dE/dx, r_{cyl} and the initial distribution of atomic velocities are used. The results in Fig. 1 show that the yield exhibits a steep ''threshold'' for $E_{\rm exc} \lesssim 2U$ and the yield becomes nearly linear in dE/dx at high dE/dx for fixed $r_{\rm cyl}$. The size of the yield in the latter regime is roughly proportional to $r_{\rm cyl}^n$ with[2] $n \sim 0.8$. This is unlike the spike models which are quadratic in dE/dx at high dE/dx where they also become independent of $r_{\rm cyl}$.

At high dE/dx the MD calculations show that the energy transport is nonlinear, producing a pressure pulse, a melt, and a crater.[2,17] However, this is, surprisingly, *not* exemplified by a strong nonlinear dependence of the sputtering yield on dE/dx when the *spike radius is fixed*. That is, the steeply increasing yield with increasing dE/dx at lower dE/dx apparently cannot be sustained. Energy is removed by the radial pressure pulse and by rapid transport of energy to the surface (paper II). This is consistent with the recent results of Nordlund *et al.*,[39] where there is collective movement of atoms toward the surface for ion bombardment of Cu. At low dE/dx, the ejecta was shown in paper II to exhibit spikelike properties. Using the simple δ distribution of excitation energies and fixed $r_{\rm cyl}$, the threshold dependence in Fig. 1 is, roughly, $Y \propto [(dE/dx)^6]$. This dependence occurs when $E_{\rm exc}$ is below the effective escape energy $\sim 2U$, whereas the threshold dependence in the analytic spike models occurs at lower $E_{\rm exc} (\ll U)$. Since the spike models assumed local thermodynamic equilibrium, we also used a Maxwellian distribution of initial excitation energies with the average energy equal to $E_{\rm exc}$. Whereas the Maxwellian and the δ distribution give the same yields at high dE/dx, the dependence in the MD threshold regime is modified. In fact, the calculated dependence is reproduced by analytic spike models such as that by Sigmund and Claussen.[3] This model also gives the correct size of the yield, although the energy transport to the surface is not included nor is the surface disruption.

In spike models, the cylindrical region associated with an ion's track is typically assumed to be excited uniformly along its length at each dE/dx. However, at low dE/dx excitations or momentum transfer events produced by a fast ion are, generally, sparsely distributed. Therefore, a more realistic description of the cylindrically energized region at low dE/dx for many relevant energy-deposition distributions is obtained by using a fixed mean $E_{\rm exc}$ and increasing the density of events with increasing[14] dE/dx. Such a distribution of energizing events was examined here. Our results for the yield at low dE/dx were shown to evolve smoothly onto the high dE/dx regime *for* those *track radii* suggested to be appropriate to electronic sputtering of low-temperature O_2 and N_2. Therefore, the observed nonlinearities in the yield[14,9] must be due to the conversion of deposited energy into atomic motion or to a variable $r_{\rm cyl}$. At the ion energies appropriate to the O_2 and N_2 sputtering data the size of the track of *initial excitations* in fact *decreases*[2] with dE/dx. However, if at high dE/dx the effective $r_{\rm cyl}$ at the time of the nonradiative decay processes *increases* with dE/dx due to excited-state transport (e.g., $r_{\rm cyl} \propto dE/dx$), the nearly quadratic dependence of Y on dE/dx observed experimentally can be reproduced.

The results here and in paper II indicate that there are three distinct energy density regimes for sputtering of atomic solids by a fast ion: low dE/dx where the yield is linear in dE/dx due to the sparse distribution of energetic events; intermediate dE/dx where the yield can be steeply varying and spikelike; and high dE/dx where the yield saturates and again becomes nearly linear due to the formation of a melt and the removal of energy by the pressure pulse. The relative importance of these regimes depends on the size of $r_{\rm cyl}$. For cases shown in Fig. 2 ($r_{\rm cyl} \lesssim 2\sigma$), the low- and high-energy regimes roughly merge, giving a nearly linear yield over all dE/dx studied. For much larger $r_{\rm cyl}$, appropriate for collision cascade sputtering by heavy ions,[3] the three regimes are distinct.

The laboratory measurements for electronic sputtering of condensed-gas solids[14,9] and for knock-on sputtering of refractory materials[40–42] show clear linear to nonlinear transitions in the yield in going from low to high dE/dx. In electronic sputtering, the nonlinearities could be due to the conversion of the deposited energy into atomic motion following the ion production of a track of excitations.[2] However, this cannot be the case for knock-on sputtering. It has been pointed out that the size of the excited region changes with the energy of the projectile in both the electronic regime[43–45] and in the nuclear regime.[46–48] This is particularly important for knock-on sputtering due to cluster bombardment.[41,42] Therefore, the radial distributions in the deposited energy in both electronic and knock-on sputtering must be treated carefully to determine the local energy density and, thereby, the appropriate sputtering regime.

ACKNOWLEDGMENTS

We acknowledge helpful comments from H.M. Urbassek and K.M. Nordlund. This work was carried out while M. Jakas was a visiting faculty at the University of Virginia. The work was supported by the NSF Divisions of Astronomy and Chemistry.

APPENDIX A: SPIKE SPUTTERING OF Cu

Energy, angle, radial, and depth distributions like those in paper I for Ar are shown in Fig. 4 for sputtering of Cu using $E_{\rm exc} = 6U$ in the cylindrical spike geometry and calculated with Morse potentials. All distributions are normalized to 1, and the angle θ is measured with respect to the surface normal. The distributions look similar to the ones in Fig. 15 of paper II for solid Ar having a cascadelike behavior in the energy distribution but with an angular distribution closer to $\cos^2 \theta$.

APPENDIX B: MAXWELLIAN VS DELTA DISTRIBUTIONS

In paper II we described the properties of the ejecta using the δ distribution. In this appendix we show how these change when a Maxwellian distribution is used as in a true thermal spike. Two scenarios were studied in detail. One in the threshold regime, $E_{\rm exc} = 0.5U$, and the other in the high-energy regime, $E_{\rm exc} = 4U$. More than 80 initially different distributions had to be considered for the Maxwellian excitation, in order for the average for particles in, for example, the surface layer to be represented by a smooth Maxwellian. The Gaussian distributions in each direction were generated

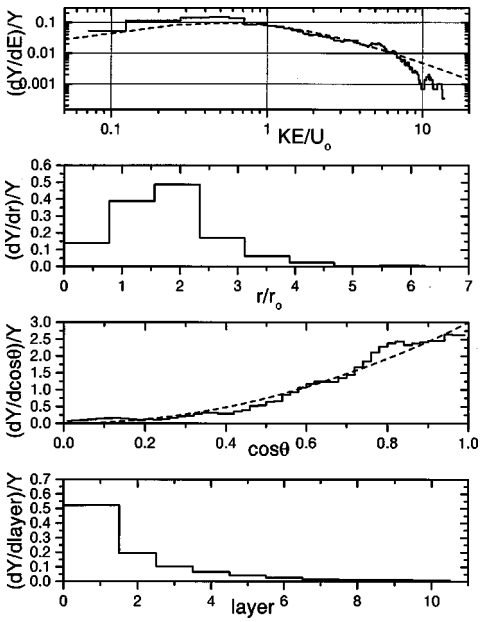

FIG. 4. Energy, angular, depth, and radial distributions of ejected particles for Cu in the nonlinear energy transport regime $E_{\rm exc}=6U$ and $N_{\rm exc}=12$. The energy distribution includes a Thompson distribution, $2UE_{\rm exc}/(E_{\rm exc}+U)^3$ (dashed line), and the angular distribution includes a $\cos^2\theta$ distribution (dashed line).

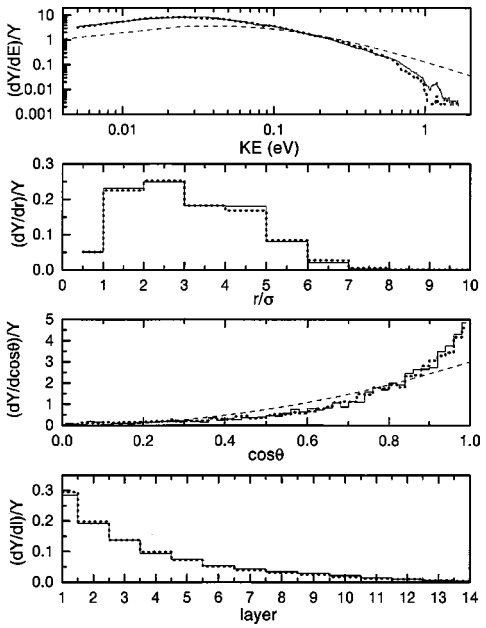

FIG. 5. Energy, radial, depth, and angular distributions for $E_{\rm exc}=4U$ and $r_{\rm cyl}=5\sigma$. Initial Maxwellian distribution (full line), and initial δ distribution (dotted line). The energy distribution includes a Thompson distribution (dashed line), and the angular distribution includes a $\cos^2\theta$ distribution (dashed line).

using the Box-Muller method.[49] A large radius, $r_{\rm cyl}=5\sigma$, with 62 excited particles per layer was chosen to improve statistics. Table III shows the main parameters of the simulation.

Energy, radial, depth, and angular distributions of the ejecta for $E_{\rm exc}=4U$, in the high-energy regime, are seen in Fig. 5. All distributions are normalized to unity, with the angle measured from the normal to the surface. The results are almost the same for both δ and Maxwellian distributions, since quasiequilibration takes a fraction of a ps. The energy distribution for the Maxwellian case has a slightly longer tail due to particles in the tail of the initial energy distribution that escaped immediately after excitation. A Thompson distribution is included for comparison.[50] The other distributions are the same within the uncertainties of the simulation. A $\cos^2\theta$ distribution is also included for comparison together with the MD angular distributions.

Energy, radial, depth, and angular distributions for $E_{\rm exc}=0.5U$, in the low-energy regime, are seen in Fig. 6. For the ''δ'' excitation the atoms require collisional energy transfer before they have enough energy to overcome the potential energy barrier. Only 9% of the ejected atoms have final energies above $E_{\rm exc}$. When the initial distribution is Maxwellian, the particles in the tail of the initial energy distribution can readily escape, the yield goes up, and 25% of the ejected atoms have final energies above $E_{\rm exc}$. The energy distribution shows this shift. From the radial distribution for δ excitation, only particles well inside the cylinder that do not lose energy by collision with cold particles escape. On the other hand, for Maxwellian excitation particles at the border of the

TABLE III. Parameters used in the simulation of Maxwellian distribution, for different $E_{\rm exc}$. Sample size (fcc cells, and number of atoms), time after excitation at which the simulation was ended, $t_{\rm end}$, and yields for Maxwellian distribution and δ distribution.

$E_{\rm exc}/U$	0.5	0.8	4
$E_{\rm exc}$ (eV)	0.04	0.064	0.32
dE/dx (eV/Å)	0.92	1.47	7.3
Size (cells)	22×22×10	22×22×10	27×27×16
Size (atoms)	19,360	19,360	46,659
$t_{\rm end}$ (ps)	20	20	50
Y_M	1.1±0.2	11.5±1.0	292±15
Y	0.32±0.12	8.5±1.5	280±15

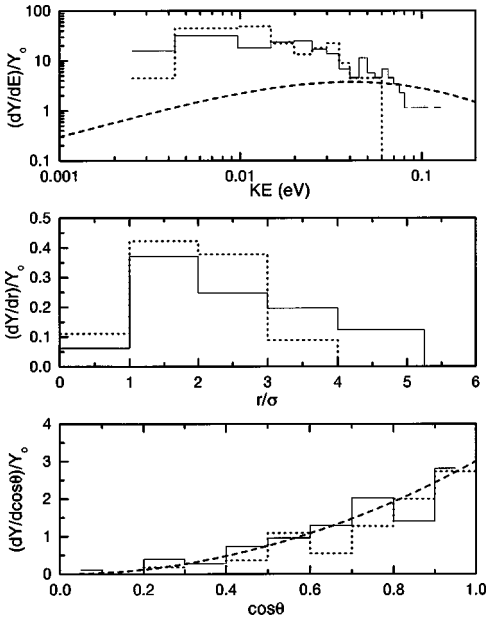

FIG. 6. Same as Fig. 5 for $E_{\rm exc}=0.5U$.

excited cylinder can still escape or are energetic enough to collisionally eject initially cold particles. Only particles from the first layer are ejected for the δ excitation case, while 2.5% of the ejecta come from the second layer for the Maxwellian excitation at this low $E_{\rm exc}$.

It is important to notice that even at $E_{\rm exc}=0.5U$ the surface is highly disrupted, and a quasifluid volume is created. Several atoms migrate to the surface were they remain as stable adatoms. There is a late ''thermal'' yield (atoms detected after 10 ps) that accounts for roughly 10% of the total yield. For instance, after two loosely attached atoms collide on top of the surface, one can go back to the solid while the other escapes. The effective binding energy can be much smaller than the initial surface binding energy.

APPENDIX C: INDIVIDUAL EXCITATIONS

When only one particle is energized in a sample of thickness $N_{\rm max}l$, where $N_{\rm max}$ is the number of layers, $Y_N(E_{\rm exc})$ is the average yield produced by an energy release $E_{\rm exc}$, in a random direction in layer N. The spatially averaged yield is $Y=\Sigma_N f_N Y_N$, where f_N is the probability of producing an excitation in layer N. If f_N is a constant and $Y_{N>N_{\rm max}}\approx 0$, MD calculations have shown that $\Sigma_N Y_N$ has a dependence on $E_{\rm exc}$ like that for a linear cascade: $\Sigma_N Y_N \approx C E_{\rm exc}/U$.[33,22] The parameter C depends weakly on the interaction potential, $C\approx 0.28$ for LJ Ar.[23]

To calculate the yield at low dE/dx for comparison to experiment we use λ, the mean free path for producing excitation events. For constant f_N, $f_N=l/\lambda$ (or in an amorphous solid or for a random crystal orientation use l/λ with $l=n^{-1/3}$), giving an average yield, $Y=(l/\lambda)\Sigma_N Y_N$. Calling $dE/dx=E_{\rm exc}/\lambda$, the energy release per unit path length, which we presume is proportional to the tabulated stopping power, we obtain Eq. (4.1). The yield is often written as $Y=\overline{\Delta z}/\lambda$ (or $\overline{\Delta x}/\lambda$), where $\overline{\Delta z}$ is a sputter depth ($\overline{\Delta z}/l=\Sigma_N Y_N \approx C E_{\rm exc}/U$).[8]

[1] E. M. Bringa and R. E. Johnson, Nucl. Instrum. Methods Phys. Res. B **143**, 513 (1998).

[2] E. M. Bringa, R. E. Johnson, and Ł. Dutkiewicz, Nucl. Instrum. Methods Phys. Res. B **152**, 267 (1999).

[3] P. Sigmund and C. Claussen, J. Appl. Phys. **52**, 990 (1981); P. Sigmund and M. Szymonski, Appl. Phys. A: Solids Surf. **33**, 141 (1984).

[4] R. E. Johnson and R. Evatt, Radiat. Eff. **52**, 187 (1980).

[5] H. Urbassek, Radiat. Eff. Defects Solids **142**, 439 (1997).

[6] A. Miotello and R. Kelly, Nucl. Instrum. Methods Phys. Res. B **122**, 458 (1997).

[7] A. Meftah *et al.*, Phys. Rev. B **49**, 12 457 (1994); J. M. Constantini, F. Brisard, M. Toulemonde, and F. Studer, Nucl. Instrum. Methods Phys. Res. B **122**, 514 (1997); G. Szenes, *ibid.* **116**, 141 (1996).

[8] R. E. Johnson and J. Schou, Mat. Fys. Medd. K. Dan. Vidensk. Selsk. **43**, 403 (1993).

[9] O. Ellegaard, J. Schou, B. Stenum, H. Sørensen, and P. Børgensen, Surf. Sci. **167**, 474 (1986).

[10] O. Ellegard, J. Schou, and H. Sørensen, Europhys. Lett. **12**, 459 (1990); O. Ellegaard, J. Schou, B. Stenum, H. Sørensen, and R. Pedrys, Nucl. Instrum. Methods Phys. Res. B **62**, 447 (1992).

[11] G. Zimmerer, Nucl. Instrum. Methods Phys. Res. B **91**, 601 (1994).

[12] R. E. Johnson, Rev. Mod. Phys. **68**, 305 (1996).

[13] W. L. Brown, L. J. Lanzerotti, and R. E. Johnson, Science **218**, 525 (1982); K. M. Gibbs, W. L. Brown, and R. E. Johnson, Phys. Rev. B **38**, 11 001 (1988).

[14] R. E. Johnson, M. Pospieszalka, and W. L. Brown, Phys. Rev. B **44**, 7263 (1991).

[15] H. M. Urbassek, H. Kafemann, and R. E. Johnson, Phys. Rev. B **49**, 786 (1994).

[16] M. Jakas, Rad. Eff. Defects Solids (to be published).

[17] In the web site: http://dirac.ms.virginia.edu/~emb3t/research/.html a number of movies can be found representing the cases treated in the paper. The movies include coordinates and velocities of the atoms.

[18] H. M. Urbassek and P. Sigmund, Appl. Phys. A: Solids Surf. **35**, 19 (1984).

[19] S. Banerjee, R. E. Johnson, S. Cui, and P. T. Cummings, Phys. Rev. B **43**, 12 707 (1991).

[20] D. Fenyö and R. E. Johnson, Phys. Rev. B **46**, 5090 (1992).

[21] R. E. Johnson, B. U. Sundqvist, A. Hedin, and D. Fenyö, Phys. Rev. B **40**, 49 (1989).

[22] S. Cui, R. Johnson, and P. T. Cummings, Surf. Sci. **207**, 186 (1988).

[23] E. M. Bringa, Nucl. Instrum. Methods Phys. Res. B **153**, 64 (1999).

[24] S. Cui, P. T. Cummings, and R. Johnson, Surf. Sci. **222**, 491 (1989).

[25] S. Banerjee, Min Liu, and R. E. Johnson, Surf. Sci. Lett. **255**, L504 (1991); R. E. Johnson and M. Liu, J. Chem. Phys. **104**, 6041 (1996).

[26] L. A. Girifalco and V. G. Weizer, Phys. Rev. **114**, 687 (1959).

[27] *Rare Gas Solids*, edited by M. L. Klein and J. A. Venables (Academic Press, New York, 1976).

[28] W. L. Brown and R. E. Johnson, Nucl. Instrum. Methods Phys. Res. **198**, 103 (1982).

[29] Mai Ghaly and R. Averback, Phys. Rev. Lett. **72**, 364 (1994).

[30] GULP, from Julian Gale, can be found at http://www.ch.ic.ac.uk/gale/Research/gulp.html

[31] M. Gsänger, H. Egger, and E. Lüscher, Phys. Lett. **27A**, 695 (1968).

[32] R. M. J. Cotteril and M. Doyama, Phys. Rev. **145**, 465 (1965); *Lattice Deffects and their Interactions*, edited by R. R. Hasiguti (Gordon and Breach, London, 1965), pp. 2–78.

[33] B. J. Garrison and R. E. Johnson, Surf. Sci. **148**, 388 (1984).

[34] R. E. Johnson, in *Ionization of Solids by Heavy Particles*, edited by R. A. Baragiola (Plenum, New York, 1993).

[35] R. Averback and T. Diaz de la Rubia, in *Solid State Physics*, edited by H. Ehrenreich and F. Spaepen (Academic, New York, 1998), Vol. 51, p. 281.

[36] T. Diaz de la Rubia and G. H. Gilmer, Phys. Rev. Lett. **74**, 2507 (1995).

[37] M. Shapiro and T. Tombrello, Nucl. Instrum. Methods Phys. Res. B **84**, 453 (1994).
[38] S.J. Zhou, D.M. Beazley, P.S. Lomdahl, and B.L. Holian, Phys. Rev. Lett. **78**, 479 (1997).
[39] Kai Nordlund, J. Keinonen, Mai Ghaly, and R. Averback, Nature (London) **398**, 49 (1999).
[40] H. H. Andersen, Mat. Fys. Medd. K. Dan. Vidensk. Selsk. **43**, 127 (1993).
[41] A. Brunelle, Nucl. Instrum. Methods Phys. Res. B (to be published).
[42] H. H. Andersen *et al.*, Phys. Rev. Lett. **80**, 5433 (1998).
[43] J. A. M. Pereira, I. S. Bitensky, and E. Da Silveira, Int. J. Mass Spectrom. Ion Processes **174**, 179 (1998).
[44] Mefta *et al.*, Nucl. Instrum. Methods Phys. Res. B (to be published).
[45] C. Watson and T. Tombrello, Radiat. Eff. **89**, 263 (1985).
[46] T. J. Colla and H. M. Urbassek, Nucl. Instrum. Methods Phys. Res. B (to be published).
[47] M.H. Shapiro and T.A. Tombrello, Nucl. Instrum. Methods Phys. Res. B **152**, 221 (1999).
[48] P. Sigmund, Nucl. Instrum. Methods Phys. Res. B.
[49] M. P. Allen and D. J. Tildesley, *Computer Simulation of Liquids* (Clarendon, New York, 1987).
[50] P. Sigmund, Phys. Rev. **184**, 383 (1969).